19th Brazilian Congress of Thermal Sciences and Engineering
November 06th-10th, 2022, Bento Gonçalves - RS - Brazil

ENC-2022-0334
STUDY OF A HYBRID CYCLE WITH A HIGH-TEMPERATURE FUEL CELL AND A THERMAL ENGINE

Davi Henrique Tomé Kannoa Vieira
Graduate Program in Mechanical Engineering, School of Mining, Federal University of Ouro Preto. Campus Morro do Cruzeiro, S/N, Bauxita, Ouro Preto, MG, Brazil. ZIP: 35400-000
davi.kannoa@aluno.ufop.edu.br

Elisângela Martins Leal
Department of Mechanical Engineering, School of Mining, Federal University of Ouro Preto. Campus Morro do Cruzeiro, S/N, Bauxita, Ouro Preto, MG, Brazil. ZIP: 35400-000
elisangelamleal@ufop.edu.br

Abstract. *In the last years, the research and development activities in fuel cell technology have been intensified within industry, research institutes and universities. As a result, fuel cells are now moving towards commercial readiness, or expecting a breakthrough within the next few years. System studies indicate that fuel cell/gas turbine hybrid system could realize a 25 percent increase in efficiency compared to the fuel cell alone. The synergy between the fuel cell and a thermal engine derives primarily from the use of the rejected thermal energy and the fuel from a fuel cell to drive the thermal engine. This paper shows an energy and exergy analyses of a solid oxide fuel cell (SOFC) coupled to a gas turbine (GT) hybrid system varying the location of the reforming system. The hybrid system is evaluated using a computer simulation at the design point. The methodology consists of describing and detailing the main components of the hybrid cycle, such as the fuel cell, gas turbine, and reformer. The fuel cell modeling consists of determining its theoretical reversible voltage, and subtracting from it the polarization losses due to ohmic drop, concentration and activation, of each of its components. The objective of this modeling is to verify the behavior of the device at the design point and off-design point and the influence in the hybrid cycle. The reforming modeling uses equilibrium calculations to find the ranges of the inlet steam/fuel ratio in order to increase the performance of the system. The gas turbine modeling is divided into parts, according to its main constituent elements. The determination of the operating parameters occurs by applying the laws of thermodynamics. SCILAB software is used to perform the simulation of the cycle, allowing the application in terms of numerical and data analyses. After the simulation, the results are compared to those of the literature. The results showed the technical feasibility of the system.*

Keywords*: solid oxide fuel cell, gas turbine, hybrid system, energy analysis, exergy analysis.*

1. INTRODUCTION

According to the Brazilian Energy Plan 2030 (EPE, 2021), at the end of the ten-year period, it is estimated that the Internal Energy Supply will have an average growth rate of 3.0% per year and reach approximately 369 million ton of oil equivalent. The internal electricity supply evolves at an average rate of 3.6% per year, reaching 2030 with an estimated supply of 909 TWh. Therefore, in the Figure 1, the estimated percentage of renewable energies in the energy matrix remains high over the horizon, around 50%, ranging from 49% in 2021, 50% in 2025 and 48% in 2030, in line with Goal 7.2 of SDG 7 for Brazil (EPE, 2021). Particularly noteworthy is the share of “Other Renewables” ranging from 8% in 2021 to 11% in 2030, and for Natural Gas, ranging from 11% in 2021 to 14% in 2030.

The concern with using energy intelligently, taking advantage of the energy potential of a source and reducing production costs, is not new. Thus, hybrid systems are being studied as a way of harnessing energy. Hybrid systems for electricity production, according to Leal et al. (2019), are systems formed by two or more sources of energy production operating together to meet the demand of a consumer.

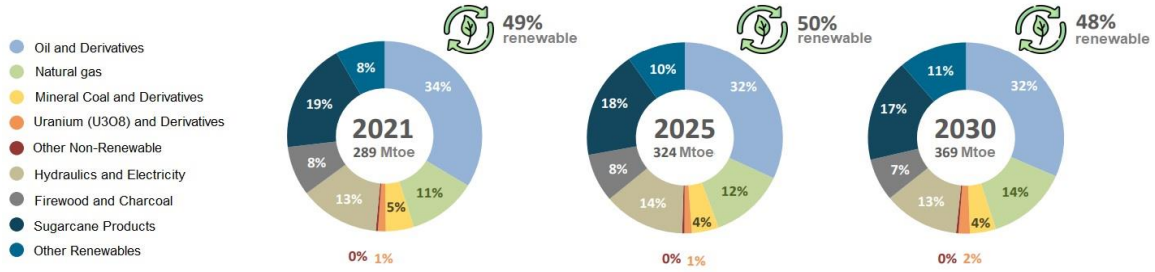

Figure 1. Estimated percentage of renewable energies in the energy matrix, to the Brazilian Energy Plan 2030 (EPE, 2021).
Note: [2]Mtoe (Million ton of oil equivalent)

The fuel cell principle has been known for over 160 years, and notwithstanding several periods of intense research and development, civil applications did not emerge until the 1990s (use in the space program has occurred since the late 1960s). According to Khaliq and Karl (2010), the main reasons are materials and production technology limitations, high costs, and the need to further improve their reliability and life.

2. STATE-OF-THE-ART OF HYBRID SYSTEMS USING FUEL CELLS

Fuel cells are commonly classified into two main groups, and are named after their electrolyte material: (1) Low-temperature fuel cells operating at temperatures lower than 300 °C such as polymer electrolyte membrane or proton exchange membrane (PEMFC), alkaline (AFC), direct methanol (DMFC), and phosphoric acid (PAFC) fuel cells. (2) High-temperature fuel cells operating at temperatures over 600 °C such as molten carbonate (MCFC) and solid oxide (SOFC) fuel cells. The different fuel cell types are shown in Table 1 along with operating temperatures and fuel cell efficiency (Khaliq; Karl, 2010).

Table 1. Types of Fuel Cells (Khaliq; Karl, 2010).

Fuel Cell	Electrolyte	Operating temperature (ºC)	Electrical efficiency (%)
DMFC	Direct methanol	50 – 120	~ 30
PEMFC	Proton exchange membrane	80 – 120	~ 30 – 35
PAFC	Phosphoric acid	100 – 220	~ 35 – 40
AFC	Alkaline	150 – 220	~ 40
SOFC	Solid oxide	600 – 1000	~ 45 – 70
MCFC	Molten carbonate	600 – 700	~ 50 – 70

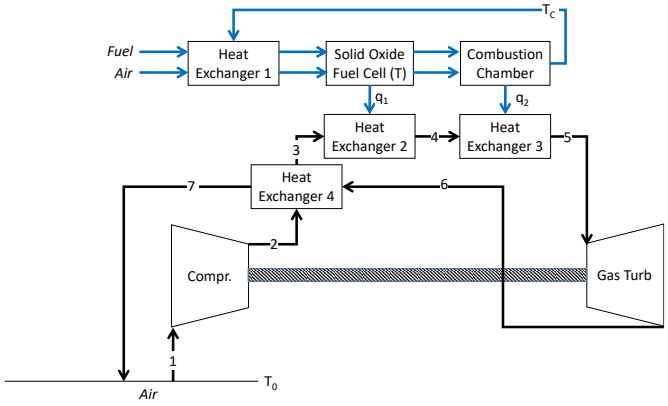

Figure 2. Schematic diagram of the SOFC–GT hybrid system (adapted from ZHANG et al., 2014)

The reforming reactions occurring in the fuel cell (directly or indirectly) or in a reforming reactor can be written as:

CO_2 reforming: $$CH_4 + CO_2 \longleftrightarrow 2\,CO + 2\,H_2 \quad (1)$$

Steam reforming: $$CH_4 + H_2O \longleftrightarrow CO + 3\,H_2 \quad (2)$$

The water gas shift (WGS) reaction can be written as:

WGS reaction: $$CO + H_2O \longleftrightarrow CO_2 + H_2 \quad (3)$$

In addition, the electrochemical reactions are:

At the anode: $H_2 + O^{2-} \rightarrow H_2O + 2\,e^-$ (4)

At the anode: $CO + O^{2-} \rightarrow CO_2 + 2\,e^-$ (5)

At the cathode: $O_2 + 4\,e^- \rightarrow 2\,O^{2-}$ (6)

3. STEAM REFORMING OF HYDROCARBONS

A very common method of hydrogen production is the steam reforming process. Usually steam reforming consists of the reaction of the fuel and steam over a catalyst to produce a mixture of H_2, CO, CO_2 and CH_4. First, a global reaction mechanism is required to analyze the thermodynamics of steam reforming of a fuel at a basic level (Ioannides, 2001; Lutz et al., 2003; Colpan et al., 2007):

Alcohols: $C_xH_yO + S(2x - 1)\,H_2O \longleftrightarrow x\,CO_2 + (2x + 0.5\,y - 1)\,H_2 + (S - 1)(2x - 1)\,H_2O$ (7)

Hydrocarbons: $C_xH_y + S(2x - 1)\,H_2O \longleftrightarrow x\,CO_2 + (2x + 0.5\,y)\,H_2 + (S - 1)(2x - 1)\,H_2O$ (8)

Where: S is the steam-to-carbon ratio. The term "global reaction" recognizes that the above reaction is actually the net result of a series of elementary reactions, some of which include catalytic interactions with surfaces. These are of no consequence to the overall thermodynamic analyses, but they are important to understand for reactor design and efficient operation and control of reformer systems. The enthalpies of formation of the species can be added to determine the net enthalpy change as follows (Ioannides, 2001; Lutz et al., 2003; Colpan et al., 2007):

Alcohols: $$\Delta H_R = x\,h^f_{CO_2} + (S-1)(2x-1)h^f_{H_2O(g)} - \left[h^f_{C_xH_yO} + S(2x-1)h^f_{H_2O(l)}\right] \quad (9)$$

Hydrocarbons: $$\Delta H_R = x\,h^f_{CO_2} + (S-1)(2x-1)h^f_{H_2O(g)} - \left[h^f_{C_xH_y} + S(2x-1)h^f_{H_2O(l)}\right] \quad (10)$$

Where: ΔH_R is the net enthalpy change in the reaction [kJ], h^f_k is the enthalpy of formation per mole of species k at standard temperature and pressure [kJ/mol].

There are two common methods used to express chemical equilibrium. One method is based on the use of equilibrium constants, while the other is based on the minimization of the free energy under the constraints of mass and energy conservation. A typical Lagrange Multipliers technique approach. One of the disadvantages of using the equilibrium constants approach is that it is more difficult to test for the presence of condensed species in the reaction products. However, it is anticipated that solid carbon may be produced during the fuel reforming process, which can deactivate the catalytic reactions. Therefore, a method based on the minimization of free energy is normally used in fuel reforming analysis. Summarizing, for a given temperature (T) and pressure (P), the equations for species conservation, atoms conservation, and condensed species are, respectively (Leal et al.; 2019):

$$N = \sum_{k=1}^{m} N_k \quad k = 1, \cdots, m \quad (11)$$

$$b_z^0 = \sum_{k=1}^{m} a_{zk} N_k = b_z \quad z = 1, \ldots, l \quad (12)$$

$$\frac{\mu_k^0}{R_u T} + \sum_{l=1}^{t} \left(\frac{\lambda_l}{R_u T} \right) a_{lk} = 0 \quad k = m+1, \ldots, n \quad (13)$$

Where: N is the molar flow [kmol/s], b_z^0 is the number of atoms of element z in the reactants [kmol], a_{zk} is the number of atoms of element z in species k in the products [kmol], μ is the molar chemical potential of species k [kJ/kmol], λ_l is a Lagrange multiplier, and R_u is the universal gas constant [8.314 kJ/kmol K]. Equations (11) to (13) form a set of n + l equations that can be simultaneously solved for the unknowns N_k, λ_l, and N. The thermodynamic function is then solved by the Newton-Raphson method for the unknowns.

4. DESCRIPTION AND MATHEMATICAL MODELING OF THE HYBRID SYSTEM

Figure 3 shows the schematic diagram of the hybrid system modeled in this paper (Fig. 3a) and the temperature-entropy plot of the corresponding process (Fig. 3b).

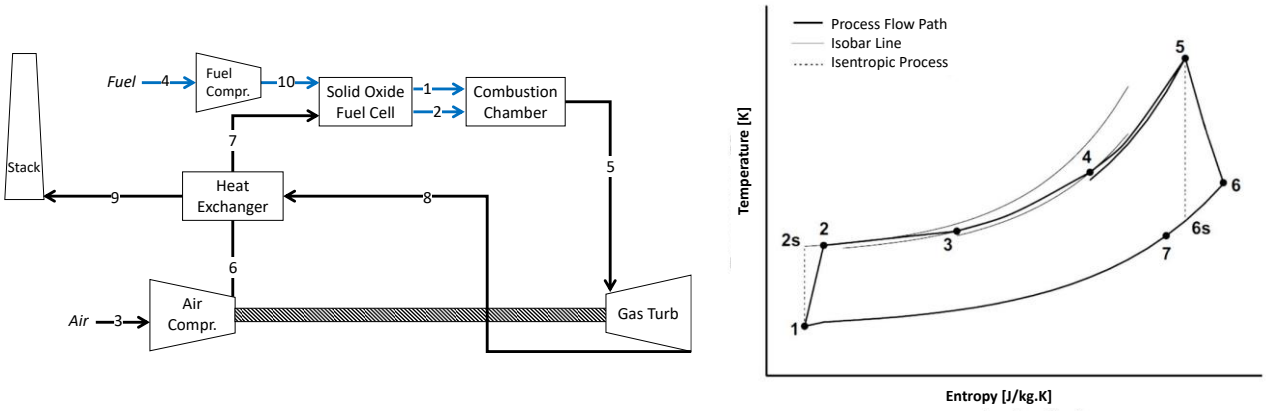

(a) Schematic of hybrid system. (b) Hybrid system temperature-entropy plot.

Figure 3. Hybrid system (a) schematic and (b) temperature-entropy plot

The first and second laws of thermodynamics are applied considering steady state of all equipment in the system and the working fluid is assumed to behave as an ideal gas. Figure 3a shows that (1) air enters the cycle through a compressor (air compressor), where it is pressurized, leaving in the state (2). Compressed air is heated by the exhaust gases (6) from the gas turbine in the heat exchanger that improves the total efficiency of the system. Thus, the heated compressed air (3) gets in the fuel cell by the cathode side to participate in the electrochemical reaction. The fuel cell has an internal reforming system, in which a pressurized fuel is used (fuel compressor) along with steam. By the electrochemical conversion, direct current power (DC power) is produced by the fuel cell. However, due to the irreversibility of such process, especially ohmic resistances, heat is generated and the temperature of the products reaches state (4). The non-oxidized fraction of the fuel is burnt in the combustion chamber of the gas turbine, located after the fuel cell. Therefore, the fuel cell products will get the desired temperature for the gas turbine entrance (5). Then, the combustion gas (5), which carries a certain amount of thermal energy, expands itself in the gas turbine in exchange for a heat loss, attaining state (6). The turbine supplies the power requirement of the compressor and provides additional power that is summed with the power provided by the fuel cell. The turbine has an axle coupled to an electric generator that produces electric power in alternating current (AC). The exhaust gases from the turbine still have some thermal energy that is used by the heat exchanger to heat up the air that will be used by the cathode of the fuel cell, reaching, thus, state (7). The exhaust gas is released through the stack.

4.1 Solid Oxide Fuel Cell – SOFC

To a hydrogen fuel cell, with known pressures of the reactants and products (Chan *et al.*, 2001):

$$\mathrm{E} = \frac{\overline{\mathrm{R}}_g\,\mathrm{T}}{2F_n}\ln \mathrm{K} - \frac{\overline{\mathrm{R}}_g\,\mathrm{T}}{4F_n}\ln\left[\frac{p_{\mathrm{H_2O}}^2\,\mathrm{P}_0}{p_{\mathrm{H_2}}^2\,p_{\mathrm{O_2}}}\right] - \frac{\boldsymbol{S}_{\mathrm{ger,vc}}\,\mathrm{T}}{2F_n} \tag{14}$$

$$\frac{\boldsymbol{S}_{\mathrm{ger,vc}}\,\mathrm{T}}{2F_n} = \Delta\mathrm{V}_{\mathrm{ativ}} + \Delta\mathrm{V}_{\mathrm{ohm}} + \Delta\mathrm{V}_{\mathrm{conc}} \tag{15}$$

According to Chan *et al*. (2001), the first term on the right side of Eq. (14) shows the effect of temperature on the fuel cell potential, while the second term shows the effect of the pressure of the reactants and products on fuel cell potential. The effect of the irreversibility on the voltage drop is considered in the third term of the Eq. (14) and it can be expressed be the activation, ohmic, and concentration polarization (Eq. 15).

Since the ionic flow of the electrolyte obeys the Ohm law, the losses by ohmic drop can be described by (Leal et al., 2019):

$$\Delta V_{ohm} = i\,R_t \tag{16}$$

$$R_t = a\,exp\left(\frac{b}{T}\right)\left(\frac{\delta}{A}\right) \tag{17}$$

Where: R_t is a total resistance of the fuel cell components, which is a temperature function, a and b are material specific constants, indicated in Table 2.

The losses due to the activation polarization in the SOFC can be described as (Virkar et al. 2000, Chan et al. 2001):

$$\Delta V_{act} = \frac{2\,R_g T}{n_e F}\sinh^{-1}\left(\frac{j}{j_0}\right) \tag{18}$$

Where j_0 is the exchange current density, that is a function of the fuel cell operating temperature and is related to the resistance of charge transfer (rtc) by:

$$j_0 = \frac{R_g T}{n_e F\, rtc} \tag{19}$$

The resistance of charge transfer can be experimentally obtained or calculated from methods in the literature. Costamagna *et al.* (1998) shows the resistance calculation from the sum of two parts: the ionic conductor resistance and the electronic conductor resistance. On the other hand, Virkar *et al.* (2000) and Tanner *et al.* (1997) show the resistance calculation from physical and electrochemical properties of the material that compose the electrode of the SOFC.

The concentration polarization can be calculated from (Leal et al., 2019):

$$\Delta V_{conc} = \frac{R_g T}{n_e F} \ln\left(1 - \frac{i}{i_L}\right) \tag{20}$$

Once all losses by polarization are calculated, the fuel cell voltage can be determined by deducting the losses by polarization from the Nernst potential. The electric energy density produced by the fuel cell can be calculated as (Chan *et al.*, 2002):

$$W_{FC} = E\, j \tag{21}$$

4.2. Gas turbine in a hybrid system

The concept of using a gas turbine in a SOFC integrated system have been well known for years. A research in the literature indicates that the concept was first analyzed by Ide *et al.* (1989), who compared three different hybrid systems in terms of net efficiency, energy generation, and energy recovery.

All the gas turbine modeling is based on Fig. 3b. The isentropic efficiency of the compressor is defined as:

$$\eta_{comp} = \frac{h_{2s} - h_1}{h_2 - h_1} \tag{22}$$

Where the ideal temperature of the working fluid at the compressor outlet can be determined using the following equation:

$$\frac{T_{2s}}{T_1} = \left(\frac{P_2}{P_1}\right)^{\frac{\gamma-1}{\gamma}} \tag{23}$$

γ is the ratio between specific heats at constant pressure (C_p) and constant volume (C_v). Applying the energy balance in the system, the work required for the compressor is:

$$\dot{W}_{comp} = \dot{m}(h_2 - h_1) \tag{24}$$

The entropy generation rate during the process of compression can be obtained from the following equation:

$$\dot{S}_{comp} = \dot{m}(s_2 - s_1) \tag{25}$$

The first law of thermodynamics for the combustion chamber can be expressed as (Cohen *et al.*, 1996):

$$\left(\dot{m}_{air,FC} + \dot{m}_{fuel,FC} U_f\right) + \dot{m}_{fuel,FC}\left(1 - U_f\right) = \dot{m}_4 = \dot{m}_5 \tag{26}$$

$$\dot{Q}_{comb} = \dot{m}_{fuel,FC}\left(1 - U_f\right) LHV \tag{27}$$

$$\dot{Q}_{loss} = \dot{m}_{fuel,FC}\left(1 - U_f\right)(1 - \eta_{cc})\, LHV$$

η_{cc} represents the efficiency of the combustion chamber. The equation of entropy balance for the combustor can be written as (Cohen *et al.*, 1996):

$$m_4 s_4 + \frac{\dot{Q}_{Comb}}{T_{Comb}} + S_{Comb} - m_5 s_5 - \frac{\dot{Q}_{Loss}}{T_\infty} = 0 \tag{28}$$

Thus, the entropy generation rate inside the combustion chamber is (Cohen *et al.*, 1996):

$$S_{Comb} = m_5 s_5 - m_4 s_4 + \frac{\dot{Q}_{Loss}}{T_\infty} - \frac{\dot{Q}_{Comb}}{T_{Comb}} = 0 \tag{29}$$

T_{Comb} refers to the adiabatic flame temperature of, in which the heat is transferred to the working fluid. As previously said, the work demanded by the compressor is provided by the gas turbine.

Knowing the turbine inlet temperature, the turbine outlet temperature can be calculated through the definition of isentropic efficiency of the gas turbine:

$$\eta_{GT} = \frac{W_{GT}}{W_{GTs}} = \frac{h_5 - h_6}{h_5 - h_{6,s}} \tag{30}$$

The gas turbine exit pressure is:

$$P_6 = P_5 \left(\frac{T_{6,s}}{T_5} \right)^{\gamma/(\gamma-1)} \tag{31}$$

The equation of entropy balance for the turbine can be obtained with (Van Wylen *et al*., 2003):

$$\dot{m}_5 s_5 - \dot{m}_6 s_6 + S_{GT} = 0 \tag{32}$$

From the mass conversion, $\dot{m}_5 s_5 = \dot{m}_6 s_6$. The entropy generation rate during the expansion process is:

$$S_{GT} = \dot{m}_5 (s_6 - s_5) \tag{33}$$

The regenerator efficiency is described as:

$$\eta_{reg} = \frac{T_3 - T_2}{T_6 - T_7} \tag{34}$$

Using the following energy balance equation, one may find the outlet temperature of the cycle:

$$\dot{m}_2 (h_3 - h_2) = \dot{m}_6 (h_6 - h_7) \tag{35}$$

Besides, the entropy balance equation for the regenerator can expressed as:

$$\dot{m}_2 s_2 + \dot{m}_6 s_6 + \dot{m}_3 s_3 + \dot{m}_7 s_7 + S_c = 0 \tag{36}$$

From the mass conservation ($\dot{m}_2 = \dot{m}_3$ and $\dot{m}_6 = \dot{m}_7$). Thus, the entropy generation rate inside the heat exchanger can be achieved with:

$$S_{reg} = \dot{m}_2 (s_3 - s_2) - \dot{m}_6 (s_6 - s_7) \tag{37}$$

4.3. Hybrid system simulation

The SOFC gas turbine hybrid system shown in Fig. 3 can be analyzed as a single control volume. The mass balance of the hybrid system can be described as:

$$\dot{m}_1 + \dot{m}_{fuel,FC} - \dot{m}_7 = 0 \tag{29}$$

$$\dot{m}_1 = \dot{m}_2 = \dot{m}_3 \tag{30}$$

$$\dot{m}_5 = \dot{m}_6 = \dot{m}_7 \tag{31}$$

The total thermal yield of the plant GT-SOFC is defined by the ratio between the net power and the total income power of the system.

$$\eta_{tot} = \left(\dot{W}_{net} / \dot{Q}_{tot} \right) \tag{32}$$

$$\dot{W}_{net} = \dot{W}_{FC,ac} + \dot{W}_{Ger} \tag{33}$$

$$\dot{W}_{FC,ac} = \eta_{inverter} \, \dot{W}_{FC,dc} \tag{34}$$

$$\dot{W}_{Ger} = \eta_{Ger} \dot{W}_{net,GT} \tag{35}$$

$$\dot{Q}_{tot} = \dot{m}_{fuel,FC} \, U_f \, LHV_{fuel} + \dot{Q}_{comb} \tag{36}$$

In which $\eta_{inverter}$ and η_{Ger} are the inverter (DC to AC) and the generator efficiency, respectively.

Table 2 indicates the physical properties of the fuel cell chosen to the present study, according to data given by the literature (Hirschenhofer *et al.,* 1994; Chan *et al.,* 2003; Virkar *et al.,* 2000; Zhu *et al.,* 2015). Table 2 information is used in the calculation of the SOFC polarization losses. Some general hypothesis have been made: the system operates in steady state; the processes are adiabatic; both the fuel cell and the regenerator operate in cross flow; the electric generator has an efficiency of 97%. Table 3 shows the system components, their identifications and the entry parameters of each equipment.

Table 2. Characteristics of the SOFC components (Hirschenhofer *et al.,* 1994; Chan *et al.,* 2003; Virkar *et al.,* 2000).

	Anode	Electrolyte	Cathode	Interconnector
Material	*Ni/YSZ*	*YSZ*	*LSM/YSZ*	*$Mg/LaCrO_3$*
Ohmic Resistance Constant	a = 0,0000298 b = -1392	a = 0,0000294 b = 10350	a = 0,0000811 b = 600	a = 0,001256 b = 4690
Thickness	$1{,}5\times10^{-4}$ m	$4{,}0\times10^{-5}$ m	$2{,}0\times10^{-3}$ m	$1{,}5\times10^{-4}$ m

Table 3. Equipment entry parameters.

Name	Parameters		
Fuel source	CH_4 or C_2H_6 or C_3H_8: 30% and H_2O: 70%. Pressure = 1.013 bar.		
Air source	N_2: 77.29%, O_2: 20.75%, H_2O: 1.01%, CO_2: 0.03% and Ar: 0.92% Pressure = 1.013 bar and Temperature = 20°C.		
Gas Turbine	η_{GT} = 0.85 / η_{GTM}= 0.99 / GT Compressor: η_{Comp} = 0.80 / r_p = 8 / η_{CM} = 0.98		
Combustor	Δ_p = 0.3bar		
Stack	P_{in} = 1.013bar		
Solid Oxide Fuel Cell	$\Delta_{p,an}$ = 0.2bar $\Delta_{p,cat}$ = 0.2bar $T_{in,an}$ = 800°C	T_{FC} = 1000°C U_f = 0.85 η_{inv} = 0.97	$R_{FC} = 5\times10^{-5}$ohm.m^2 j = 2500 A/m^2 A_{FC} = 800m^2
Regenerator	$\Delta_{p.hot}$ = 0.1 bar	$\Delta_{p.cold}$ = 0.1bar	$T_{out.cold}$ = 800°C
Fuel compressor	η_{C2} = 0.70	η_{CM2} = 0.98	r_p = 8

5. RESULTS AND DISCUSSION

SCILAB software version 6.1.1 is used to perform the fuel cell thermodynamics simulation, and the thermodynamic simulation of the hybrid system. The results obtained are generated from the hybrid cycle and is shown in tables 4, 5 and 6.

Table 4. Results for the thermodynamic simulation with the mixture of H_2O (70%) and CH_4 (30%)

Pipe no.	Mass flow [kg/s]	Pressure [bar]	Temperature [ºC]	Enthalpy [kJ/kg]	Entropy [kJ/kg.K]	Exergy [kJ/kg]
1	83.669	7.904	950.00	923.31	78.239	747.78
2	2.674	7.904	950.00	-9748.64	109.753	2928.70
3	84.963	1.013	20.00	-93.80	68.827	0.15
4	1.381	1.013	382.70	-10223.69	127.746	14931.00
5	86.343	7.604	984.98	592.76	79.960	793.87
6	84.963	8.104	311.29	205.36	69.904	268.27
7	84.963	8.004	800.00	747.94	76.652	616.39
8	86.343	1.113	581.77	115.44	80.991	286.85
9	86.343	1.013	88.88	-418.46	72.025	11.30
10	1.381	8.104	800.00	-9089.93	131.100	15968.12

Table 5. Results for the thermodynamic simulation with the mixture of H_2O (70%) and C_2H_6 (30%)

Pipe no.	Mass flow [kg/s]	Pressure [bar]	Temperature [ºC]	Enthalpy [kJ/kg]	Entropy [kJ/kg.K]	Exergy [kJ/kg]
1	83.855	7.904	950.00	923.31	78.239	747.78
2	2.273	7.904	950.00	-9193.15	102.877	3072.25
3	85.148	1.013	20.00	-93.80	68.827	0.15
4	0.980	1.013	463.71	-8015.55	114.969	21414.44
5	86.128	7.604	985.76	656.32	79.561	789.78
6	85.148	8.104	311.29	205.36	69.904	268.27
7	85.148	8.004	800.00	747.94	76.652	616.39
8	86.128	1.113	581.76	180.97	80.587	284.86
9	86.128	1.013	83.49	-355.44	71.518	9.77

10	0.980	8.104	800.00	-7040.70	117.821	22307.09

Table 6. Results or the thermodynamic simulation of the mixture of H_2O (70%) and C_3H_8 (30%)

Pipe no.	Mass flow [kg/s]	Pressure [bar]	Temperature [ºC]	Enthalpy[kJ/kg]	Entropy [kJ/kg.K]	Exergy [kJ/kg]
1	89.094	7.904	950.00	923.34	78.238	747.73
2	2.113	7.904	950.00	- 9235.23	95.137	2944.27
3	90.387	1.013	20.00	-93.80	68.827	0.15
4	0.819	1.013	549.53	-6518.10	107.432	25763.61
5	91.206	7.604	977.86	688.04	79.281	779.84
6	90.387	8.104	311.29	205.36	69.904	268.27
7	90.387	8.004	800.00	747.94	76.652	616.39
8	91.206	1.113	575.64	216.87	80.306	279.14
9	91.206	1.013	73.90	-320.84	71.067	7.67
10	0.819	8.104	800.00	-5747.32	108.901	26492.05

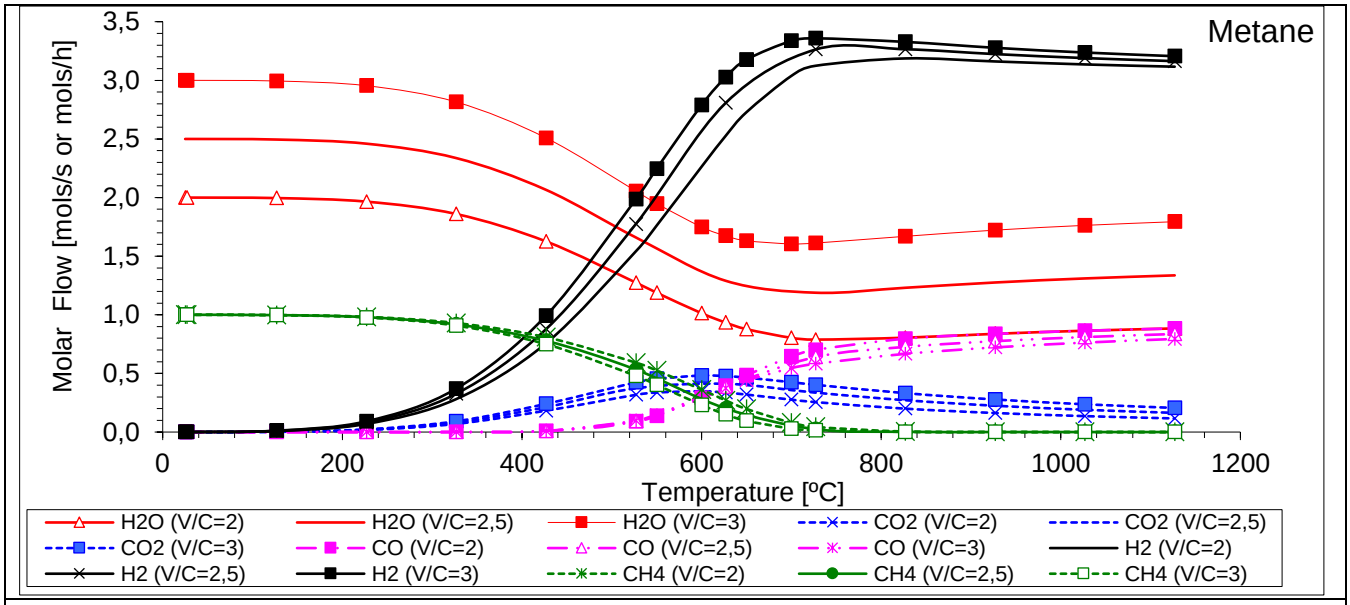

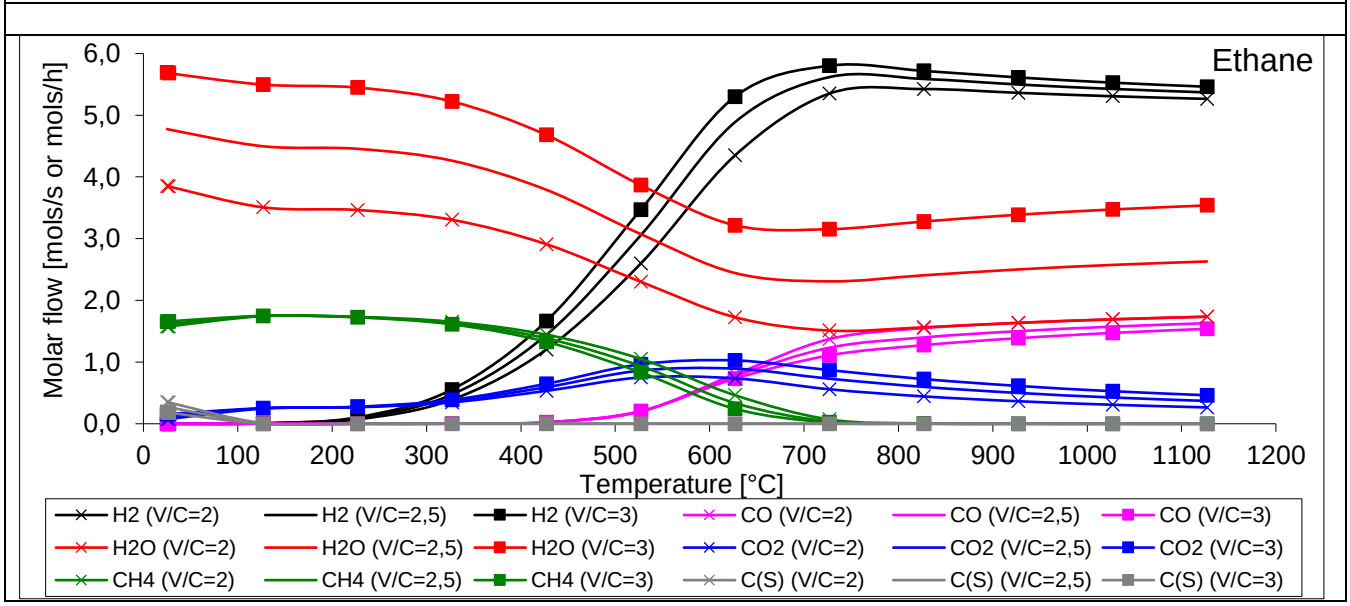

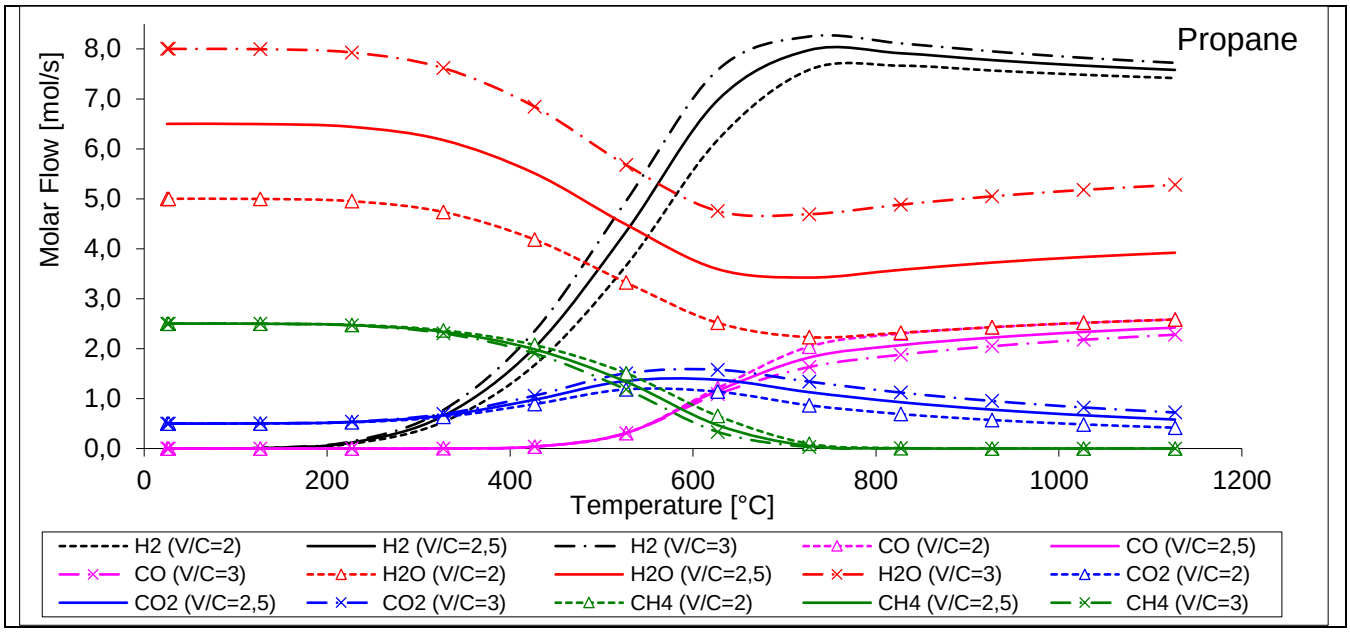

Figure 6. Results of steam reforming of CH_4, C_3H_8, and C_2H_6.

In Figure 6 is possible to see an inverse relationship between temperature and molar flow, where whereas the temperature increases, the flow velocity decreases. One of the reasons for this to happen is that substances decompose as the temperature increases, and in this process the molecules are separating and losing their structure, which directly influences the drop in flow velocity.

6. NOMENCLATURE

A - Area [m^2 or cm^2]
C_p - Specific heat at constant pressure [kJ/kg.K]
C_v - Specific heat at constant volume [kJ/kg.K]
E - Operation cell voltage [V]
F - Faraday constant [96487.309 C/mol]
h - Specific enthalpy [kJ/kg]
i - Current [A]
i_L - Limiting current [A]
j - Current density [A/m^2]
j_0 - Exchange current density [A/m^2]
K - Reaction equilibrium constant [-]
LHV - Lower heating value [kJ/kg or kJ/kmol]
$\dot{m}$ - Mass flowrate [kg/s]
n_e - Number of electrons transferred per mole of fuel [mol e^- /mol]
P - Pressure [kPa or MPa]
p_i - Partial pressure of the component *i* [kPa]
$\dot{Q}$ - Heat transfer rate [kW]
$\overline{R}_g$ - Universal gas constant [8.315 kJ/kmol.K]
r_p - Pressure ratio [-]
R_t - Total resistance of the cell components [Ω]
rtc - Resistance to charge transfer [$\Omega.m^2$]
S - Entropy [kJ/K]
s - Specific entropy [kJ/kg.K]
T - Temperature [°C or K]
U_f - Fuel utilization [-]
W_{FC} - Electric energy density [J/m^2]
W - Work [kJ]
$\dot{W}$ - Power [kW]

GREEK LETTERS

ΔV_{act} - Activation Polarization [V]
ΔV_{conc} - Concentration polarization [V]
ΔV_{ohm} - Ohmic Polarization [V]
Δ_p - Pressure drop [kPa]
δ - Equivalent thickness of the diffusion layer [m]
η - Efficiency
η_{elec} - Electric energy efficiency
η_{GT} - Isentropic efficiency of the gas turbine [-]
η_{GTM} - Mechanical efficiency of the gas turbine [-]
η_C - Isentropic efficiency of the compressor [-]
η_{CM} - Mechanical efficiency of the compressor [-]
ρ_m - Resistivity [[Ω.m]
γ - Isentropic coefficient [-]

Subscripts

0 - Standard state (1 atm and 25ºC)
ac - Alternating current
an - Anode
cat - Cathode
∞ - Environment
C - Compressor
Comb - Combustor
dc - Direct current
FC - Fuel cell
Ger - Generator
GT - Gas Turbine
reg - Regenerator

7. CONCLUSIONS

In this work, thermodynamic, energy and exergy analyzes were carried out, based on data collected, by simulations made,

of a solid oxide fuel cell (SOFC) coupled to a hybrid gas turbine (GT) system varying the location of the reform system. Three mixtures were used, with different compositions, (01) of water H_2O (70%), and propane C_3H_8 (30%) ; (02) of water, H_2O (70%), and ethane C_2H_6 (30%) ; (03) of water, H_2O (70%), and methane CH_4 (30%). And from them, simulations were carried out, collection and comparison of data generated between the three.

The results obtained from the simulation of the mixture with methane and ethane are similar, while with propane there were some differences. One of the reasons for this to happen is that substances decompose with increasing temperature, and in this process the molecules are separating and losing their structure, which directly influences the drop in flow velocity. Fuels with long carbon chains, and branched have weaker intermolecular interactions, and therefore do not need much heat, energy, to decompose. As is the case with the boiling temperatures of the three fuels.

8. ACKNOWLEDGEMENTS

The authors acknowledge the Graduate Program of Mechanical Engineering (PROPEM) at the Federal University of Ouro Preto and the Coordination of Superior Level Staff Improvement for the financial support of this work.

9. REFERENCES

Khaliq A, Föger Karl. Fuel processing for high-temperature high-efficiency fuel cells. Ind Eng Chem Res 2010;49(16):7239–56. URL http://dx.doi.org/10.1021/ie100778g.

Lutz A E; Bradshaw R W; Keller J O; Witmer D E. Thermodynamic analysis of hydrogen production by steam reforming. International Journal of Hydrogen Energy. Volume 28, Issue 2, February 2003, Pages 159-167

Colpan C O; Ibrahim Dincer; Feridun Hamdullahpur. Thermodynamic modeling of direct internal reforming solid oxide fuel cells operating with syngas. International Journal of Hydrogen Energy. Volume 32, Issue 7, May 2007, Pages 787-795

Chan S H; Khor K A; Xia Z T. A complete polarization model of a solid oxide fuel cell and its sensitivity to the change of cell component thickness. Journal of Power Sources. Vol.93, pp. 130 - 140, 2001.

Chan S H; Ho H K; Tian Y. Multi-level modeling of SOFC–gas turbine hybrid system. Int J Hydrogen Energy, v. 28, p.889–900, 2003.

Chan S H; Low C F; Ding O L. Energy and exergy analysis of simple solid-oxide fuel-cell power systems. Journal of Power Sources. Vol.103, Issue 2, pp. 188 - 200, 2002.

EPE – Energy Research Company. Brazilian National Energy Balance 2021. Ministério de Minas e Energia - MME. Available at: <https://www.epe.gov.br/sites-pt/publicacoes-dados-abertos/publicacoes/PublicacoesArquivos/publicacao-490/topico-522/Caderno%20de%20Consolida%C3%A7%C3%A3o%20dos%20Resultados.pdf> Accessed in 06/06/2022.

EG&G Services Parsons Inc. Fuel Cell Handbook (Fifth Edition). West Virginia: National Energy Technology Laboratory, U.S. Department of Energy, contract no. DE-AM26-99FT40575, 2000.

Leal, E M; L A Bortolaia, A M Leal Junior. Technical analysis of a hybrid solid oxide fuel cell / gas turbine cycle. Energy Conversion and Management, Volume 202, 2019.

Ioannides T. Thermodynamic analysis of ethanol processors for fuel cell applications, Journal of Power Sources, vol. 92(1-2), pp. 17-25, (2001).

Mclarty D; J Brouwer; S Samuelsen. Fuel cell–gas turbine hybrid system design part II: Dynamics and control. Journal of Power Sources, v. 254, p. 126–136, 2014.

Ghassemi M; Majid Kamvar; Robert Steinberger Wilckens. Fundamentals of Heat and Fluid Flow in High Temperature Fuel Cells. 2020. Available at https://www.sciencedirect.com/book/9780128157534/fundamentals-of-heat-and-fluid-flow-in-high-temperature-fuel-cells

Meng Ni. Modeling and parametric simulations of solid oxide fuel cells with methane carbon dioxide reforming. Energy Conversion and Management 70 (2013) 116–129. URL https://doi.org/10.1016/j.enconman.2013.02.008

Zhang X; Yuan Wang; Tie Liu; Jincan Chen. Theoretical basis and performance optimization analysis of a solid oxide fuel cell–gas turbine hybrid system with fuel reforming. Energy Conversion and Management 86 (2014) 1102–1109. URL https://doi.org/10.1016/j.enconman.2014.06.068

10. RESPONSIBILITY NOTICE

The authors are the only responsible for the printed material included in this paper.